Supporting Information

Revealing the composition-dependent structure evolution fundamentals of bimetallic nanoparticles through the inter-particle alloying reaction

Yingzheng Lin,[a,b] Yitao Cao,[b] Qiaofeng Yao,[*,b] and Jianping Xie[*,a,b]

[a] Joint School of National University of Singapore and Tianjin University, International Campus of Tianjin University, Binhai New City, Fuzhou 350207, P. R. China

[b] Department of Chemical and Biomolecular Engineering, National University of Singapore, 4 Engineering Drive 4, Singapore 117585, Singapore.

Experimental Section

Chemicals

Hydrogen tetrachloroaurate(III) trihydrate ($HAuCl_4 \cdot 3H_2O$), *para*-mercaptobenzoic acid (*p*-MBA), sodium borohydride ($NaBH_4$), cesium hydroxide hydrate ($CsOH \cdot H_2O$), sodium hydroxide (NaOH), acetic acid (HOAc) and N,N-dimethylformamide (DMF) from *Sigma Aldrich*; silver nitrate ($AgNO_3$) from *Merck*; ethanol and toluene from *Fisher* were used as-received without further purification. Ultrapure Millipore water (18.2 MΩ.cm) was used in preparation of all aqueous solutions.

Synthesis of $[Au_{44}(p\text{-MBA})_{26}]^{2-}$ nanoclusters (NCs)

$[Au_{44}(p\text{-MBA})_{26}]^{2-}$ was synthesized according to the reported method.[1] In a typical synthesis, 1.25 mL of 50 mM *p*-MBA ethanolic solution and 1.25 mL of 50 mM $HAuCl_4$ aqueous solution were added into 45 mL of ultrapure water. The pH of the solution was adjusted to 13.0 by adding 1 M NaOH solution, leading to the formation of a pale-yellow Au(I)-(*p*-MBA) complex solution. The complex solution was then stirred at 500 rpm for 30 min, before bubbling with CO for 2 min. The reaction was allowed to proceed at room temperature (25 °C) for 6 days. After 6 days, the raw product of $[Au_{44}(p\text{-MBA})_{26}]^{2-}$ was purified by adding ethanol (1/5 V/V), followed by centrifugation at 12,000 rpm for 5 mins. As the inter-cluster reaction will be carried out in dimethyl formamide (DMF) solution, $[Au_{44}(p\text{-MBA})_{26}]^{2-}$ NCs will be fully protonated. The precipitation of $[Au_{44}(p\text{-MBA})_{26}]^{2-}$ NCs was first dissolved in a DMF

solution containing 30% V/V acetic acid (HOAc), and then precipitated by adding toluene (1/4 V/V). In the second round, the precipitated $[Au_{44}(p\text{-MBA})_{26}]^{2-}$ NCs were dissolved in the DMF solution containing 10% V/V HOAc and further precipitated by adding toluene (1/4 V/V). The NC precipitate can be well dissolved in DMF for further reactions.

Synthesis of $[Ag_{44}(p\text{-MBA})_{30}]^{4-}$ NCs

The synthesis of $[Ag_{44}(p\text{-MBA})_{30}]^{4-}$ NCs was according to the reported method.[2] In a typical synthesis, 21 mL of 11.9 mM $AgNO_3$ aqueous solution was added to 12 mL of 83 mM *p*-MBA ethanolic solution. The pH of the solution was brought to 12.0 by dropping 50% V/V CsOH solution, leading to the formation of a clear Ag(I)-(*p*-MBA) complex solution. Afterwards, the complexes were reduced by adding 9 mL of $NaBH_4$ aqueous solution. The raw product of $[Ag_{44}(p\text{-MBA})_{30}]^{4-}$ NCs was obtained after 12 h of reaction and purified by adding ethanol (1/2 V/V), followed by centrifugation at 12,000 rpm for 5 mins. The protonation procedure of $[Ag_{44}(p\text{-MBA})_{30}]^{4-}$ NCs was the same as that of $[Au_{44}(p\text{-MBA})_{26}]^{2-}$ NCs.

Inter-cluster reaction

Stock solutions of $[Ag_{44}(p\text{-MBA})_{30}]^{4-}$ and $[Au_{44}(p\text{-MBA})_{26}]^{2-}$ with the same concentration of 0.01 mM NCs were firstly prepared. After that, an inter-cluster reaction with a specific Au/Ag ratio was carried out by mixing the corresponding volume ratio of $[Ag_{44}(p\text{-MBA})_{30}]^{4-}$ and $[Au_{44}(p\text{-MBA})_{26}]^{2-}$. For example, in the reaction

of $R_{Au44/Ag44}$ = 1/3, 1 mL of 0.01 mM $[Au_{44}(p\text{-MBA})_{26}]^{2-}$ solution was mixed with 3 mL of 0.01 mM $[Ag_{44}(p\text{-MBA})_{30}]^{4-}$.

Materials Characterization

UV-vis absorption spectra of the NC solution were recorded by a Shimadzu UV-1800 spectrometer. The concentration of the NC solution was determined by inductively coupled plasma - optical emission spectrometry (ICP-OES) on a Thermo Scientific iCAP 6000. Electrospray ionization mass spectrometry (ESI-MS) analysis was carried out on a Bruker microTOF-Q system in negative ion mode under the source temperature of 120 °C, dry gas flow rate of 4 L per min, nebulizer pressure of 0.4 bar, and capillary voltage of 3.5 kV. In a typical ESI-MS analysis, 0.2 mL of NCs in DMF (with a NC concentration of ~0.01 mM) was injected with a flow rate of 3 μL per min.

Supporting Figures

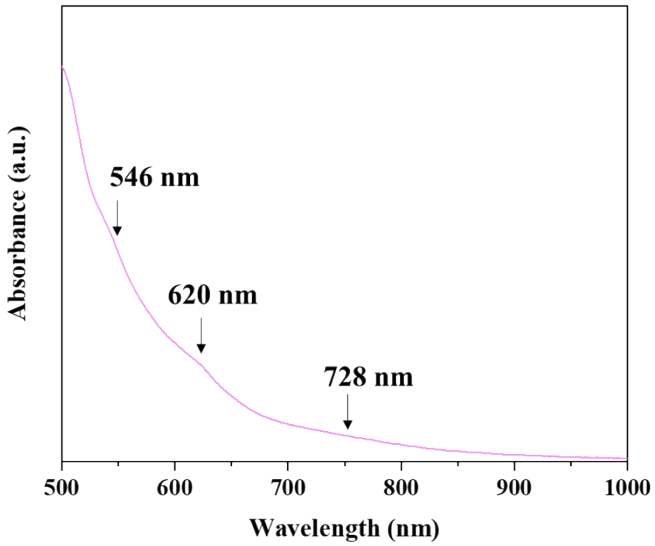

Figure S1. UV-vis absorption spectrum of the as-synthesized $[Au_{12}Ag_{32}(SR)_{30}]^{4-}$, showing three humps at 546, 620, and 728 nm.

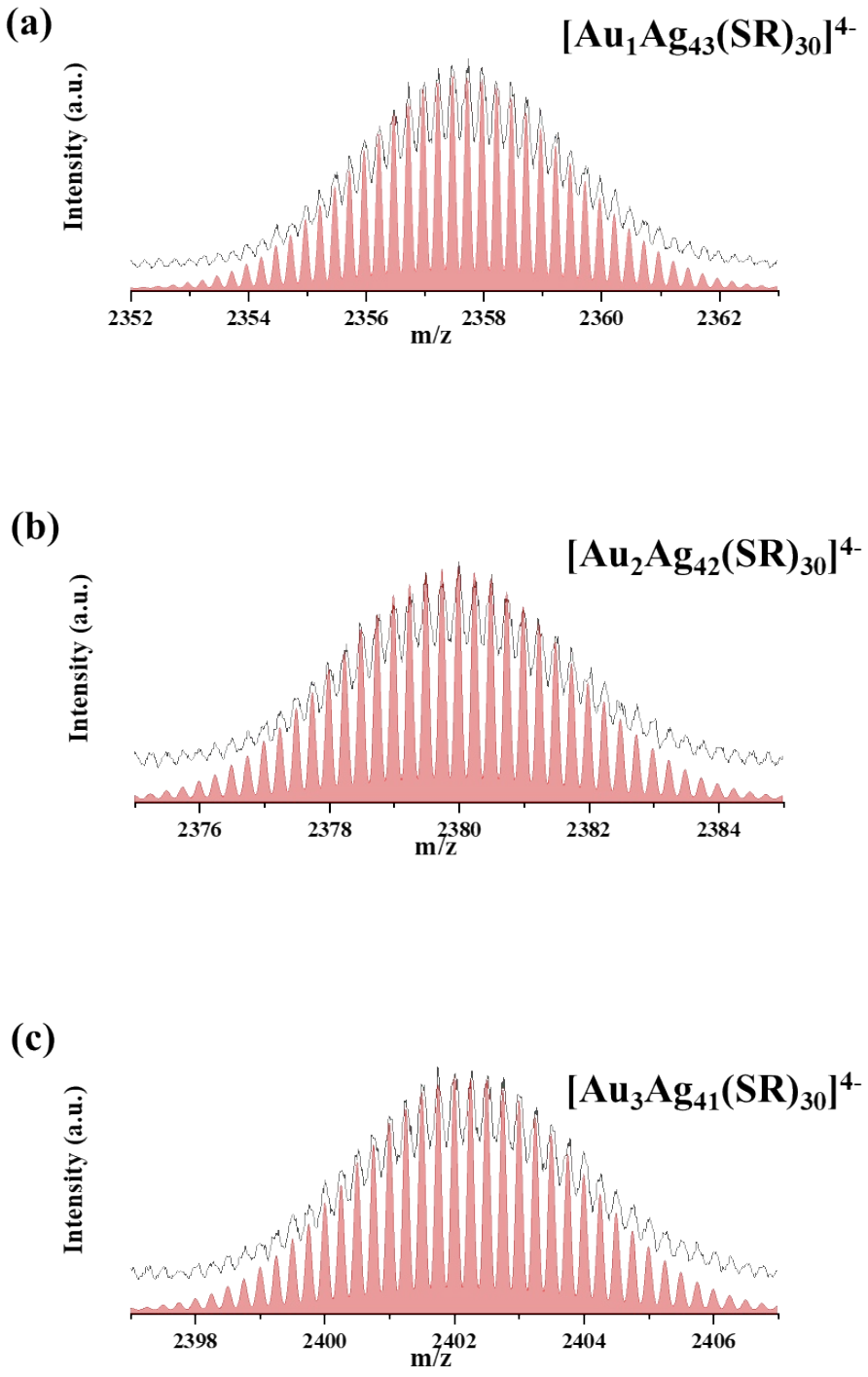
(a)
$[Au_1Ag_{43}(SR)_{30}]^{4-}$
Intensity (a.u.)
2352
2354
2356
2358
2360
2362
m/z
(b)
$[Au_2Ag_{42}(SR)_{30}]^{4-}$
Intensity (a.u.)
2376
2378
2380
2382
2384
m/z
(c)
$[Au_3Ag_{41}(SR)_{30}]^{4-}$
Intensity (a.u.)
2398
2400
2402
2404
2406
m/z

(d)

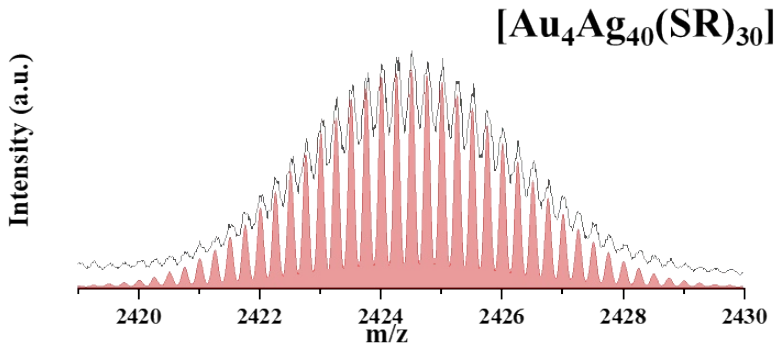
[Au4Ag40(SR)30]4-
Intensity (a.u.)
2420
2422
2424
2426
2428
2430
m/z

(e)

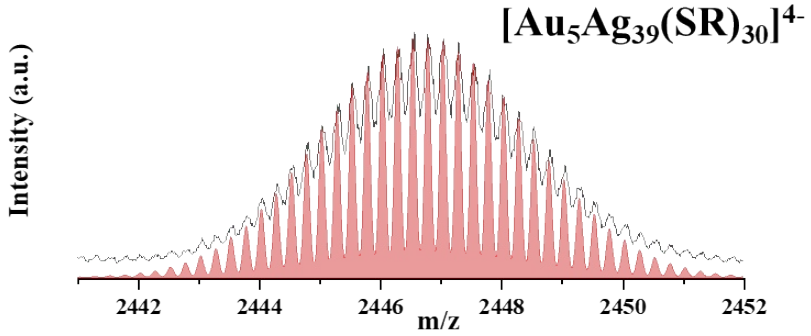
[Au5Ag39(SR)30]4-
Intensity (a.u.)
2442
2444
2446
2448
2450
2452
m/z

(f)

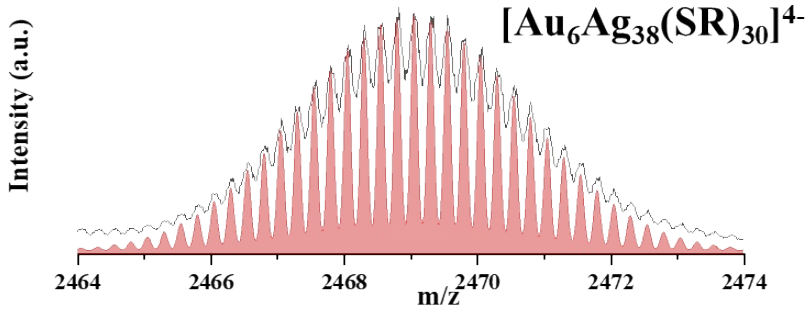
[Au6Ag38(SR)30]4-
Intensity (a.u.)
2464
2466
2468
2470
2472
2474
m/z

(g)

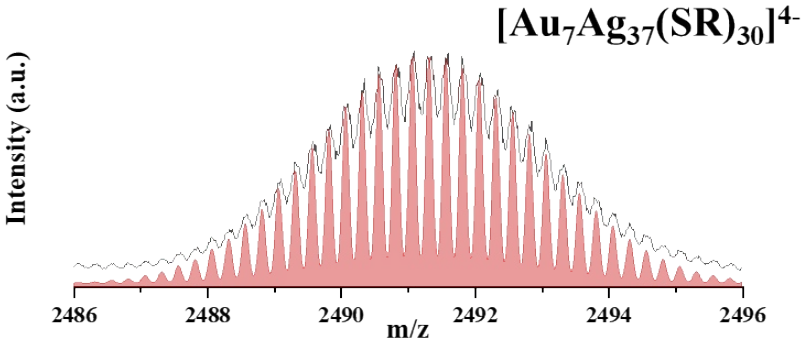
[Au7Ag37(SR)30]4-
Intensity (a.u.)
2486
2488
2490
2492
2494
2496
m/z

(h)

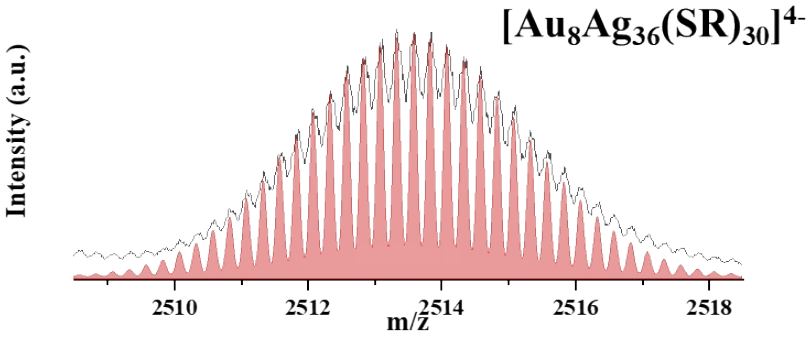
[Au8Ag36(SR)30]4-
Intensity (a.u.)
2510
2512
2514
2516
2518
m/z

(i)

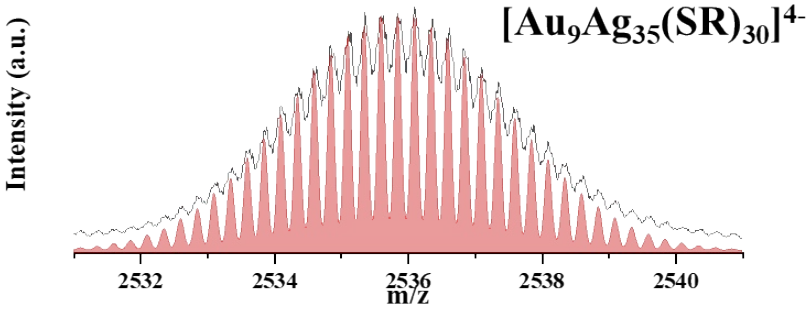
[Au9Ag35(SR)30]4-
Intensity (a.u.)
2532
2534
2536
2538
2540
m/z

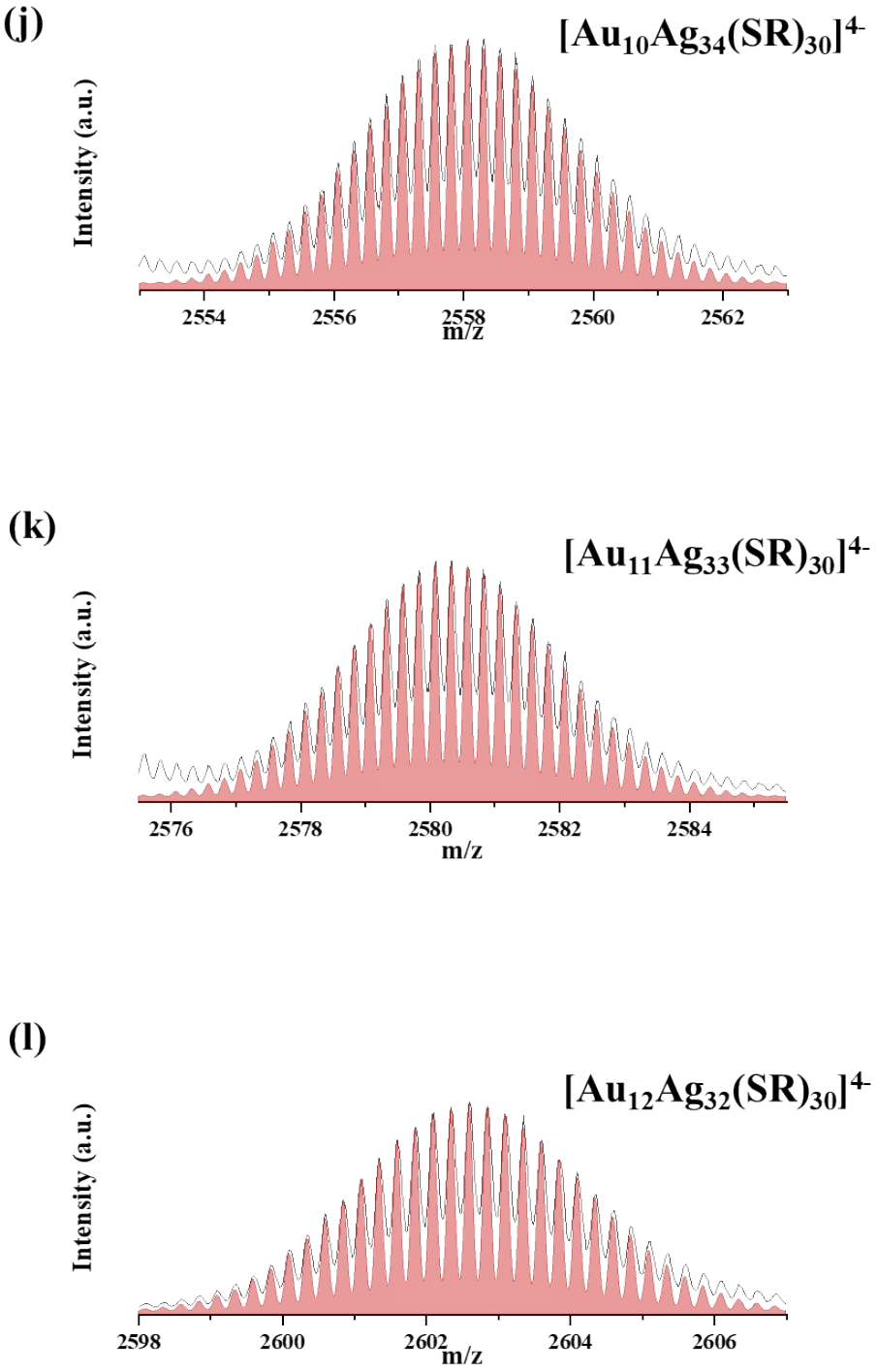

Figure S2. Experimental (black lines) and simulated (red lines) isotope patterns of $[Au_xAg_{44-x}(p\text{-MBA})_{30}]^{4-}$ (x = 1-12) NCs.

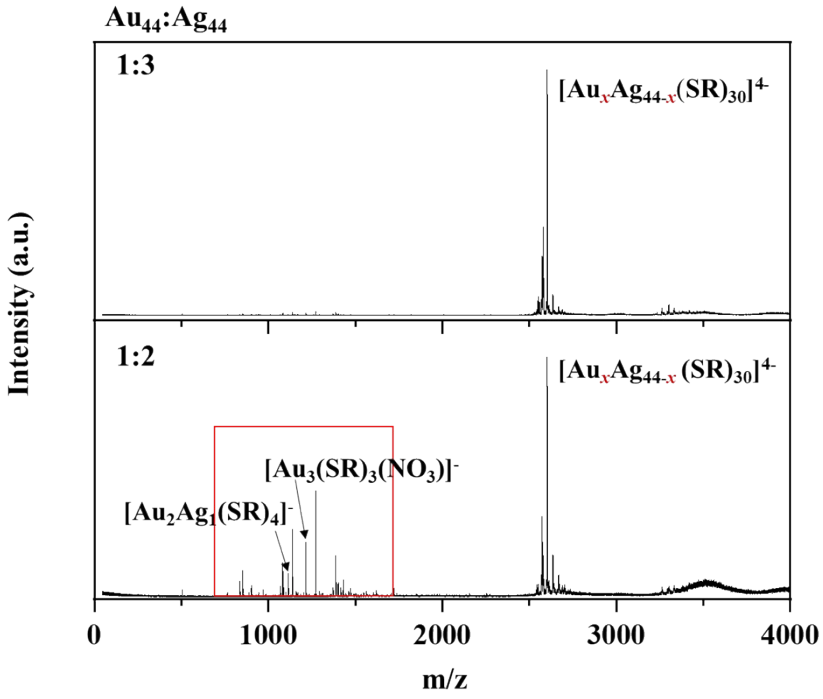

Figure S3. ESI mass spectra of alloy Au/Ag NCs synthesized at $R_{Au44/Ag44}$ = 1/3 and 1/2.

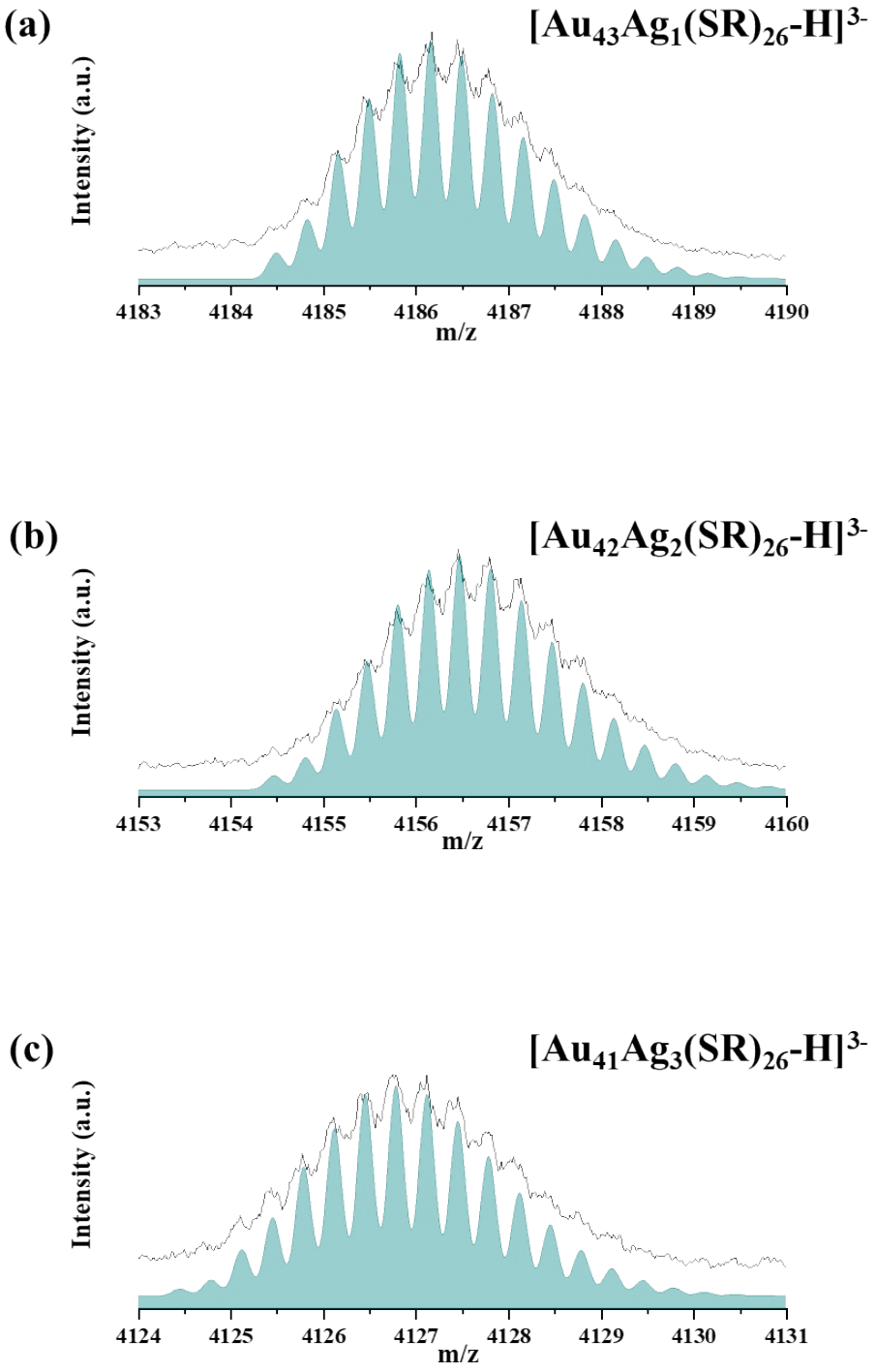
(a)
[Au43Ag1(SR)26-H]3-
Intensity (a.u.)
4183
4184
4185
4186
4187
4188
4189
4190
m/z
(b)
[Au42Ag2(SR)26-H]3-
Intensity (a.u.)
4153
4154
4155
4156
4157
4158
4159
4160
m/z
(c)
[Au41Ag3(SR)26-H]3-
Intensity (a.u.)
4124
4125
4126
4127
4128
4129
4130
4131
m/z

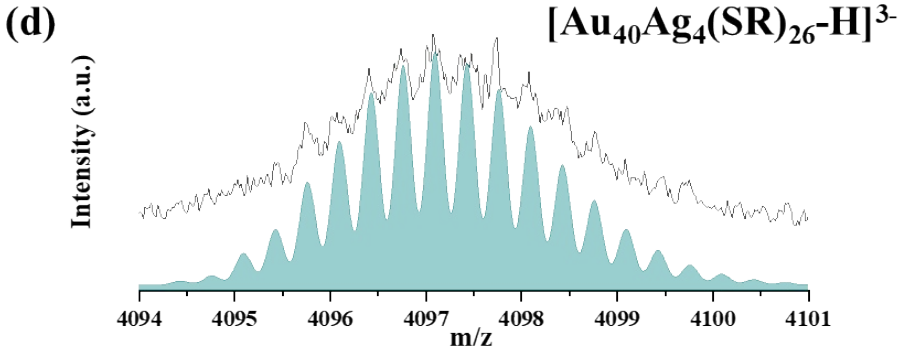
(d)
[Au40Ag4(SR)26-H]3-
Intensity (a.u.)
4094
4095
4096
4097
4098
4099
4100
4101
m/z

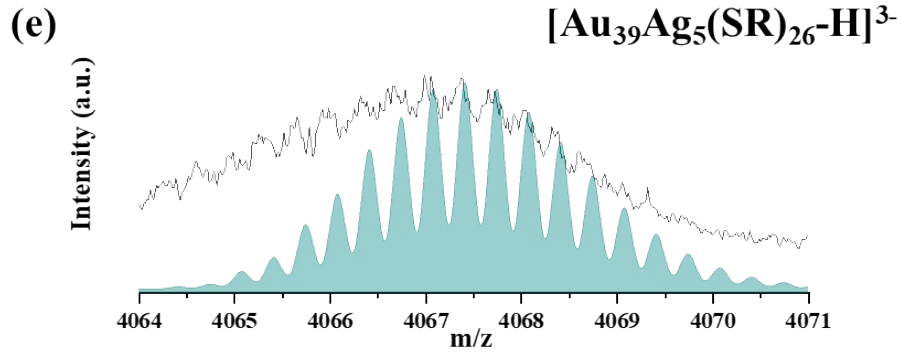
(e)
[Au39Ag5(SR)26-H]3-
Intensity (a.u.)
4064
4065
4066
4067
4068
4069
4070
4071
m/z

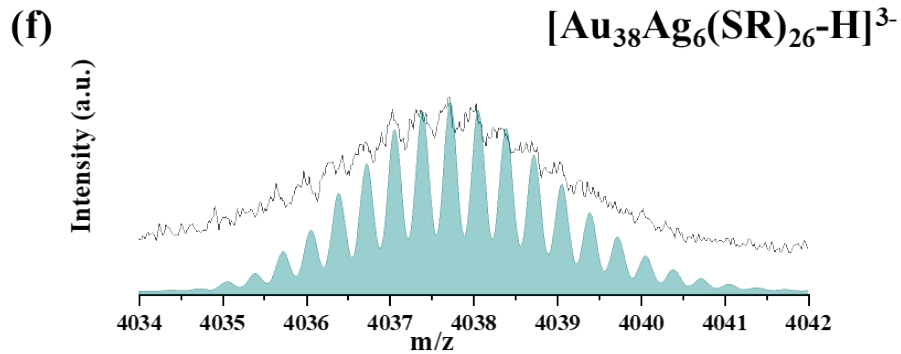
(f)
[Au38Ag6(SR)26-H]3-
Intensity (a.u.)
4034
4035
4036
4037
4038
4039
4040
4041
4042
m/z

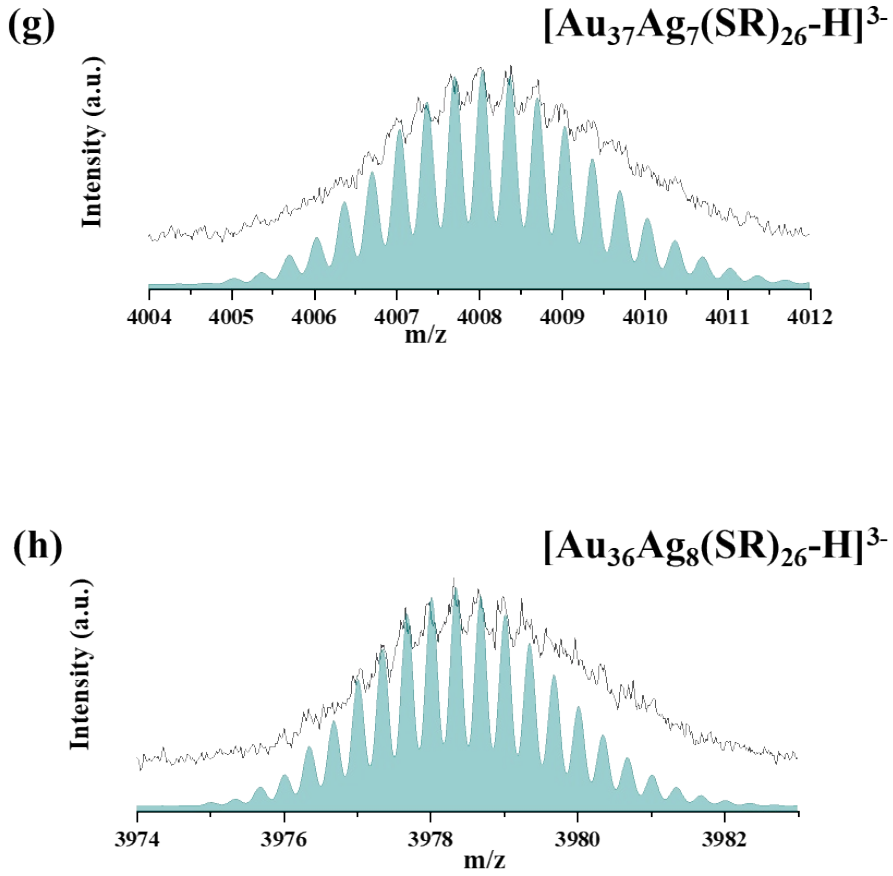

Figure S4. Experimental (black lines) and simulated (green lines) isotope patterns of $[Au_xAg_{44-x}(SR)_{26} - H]^{3-}$ (x = 36-43) NCs.

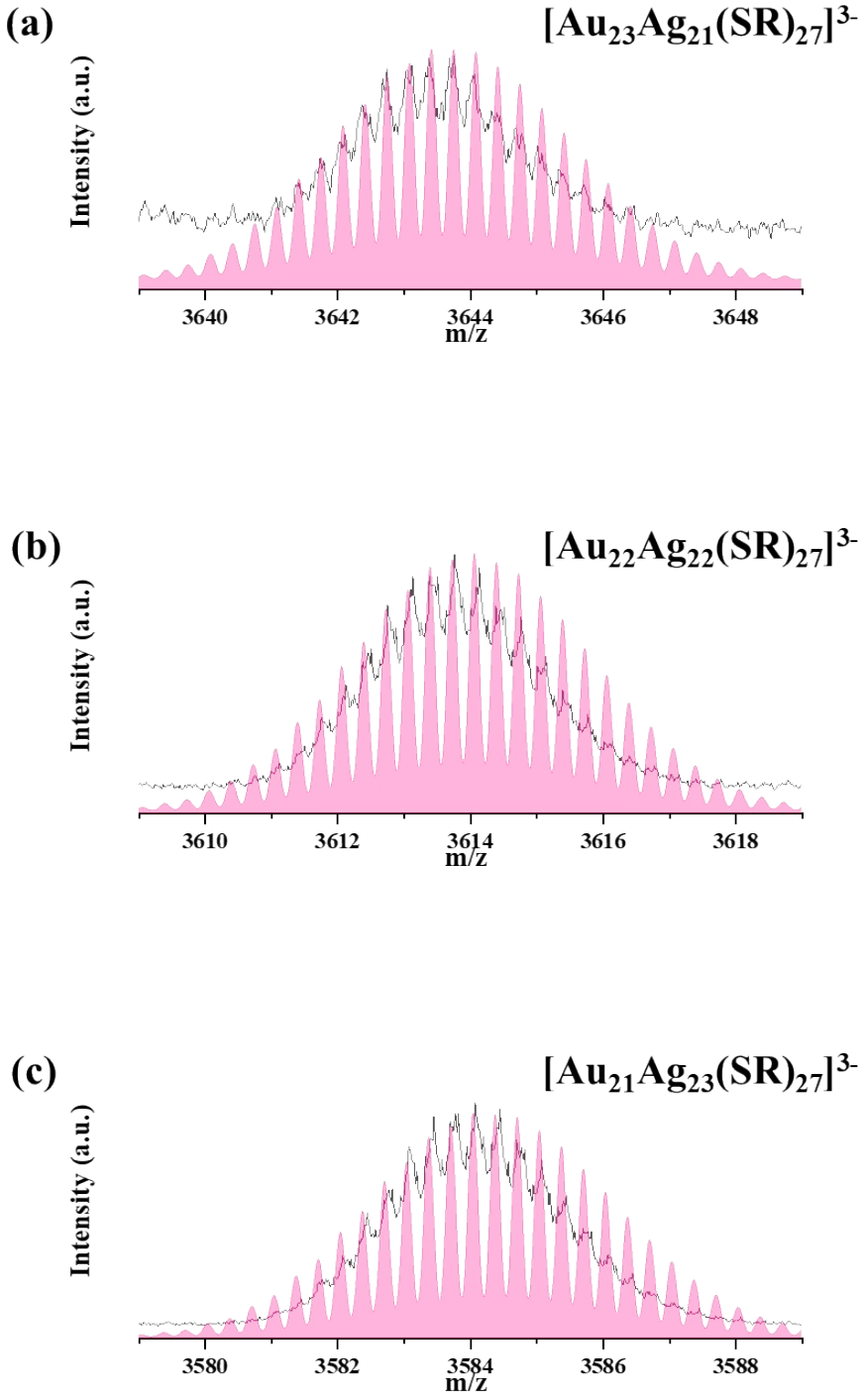
(a)
$[Au_{23}Ag_{21}(SR)_{27}]^{3-}$
Intensity (a.u.)
3640
3642
3644
3646
3648
m/z
(b)
$[Au_{22}Ag_{22}(SR)_{27}]^{3-}$
Intensity (a.u.)
3610
3612
3614
3616
3618
m/z
(c)
$[Au_{21}Ag_{23}(SR)_{27}]^{3-}$
Intensity (a.u.)
3580
3582
3584
3586
3588
m/z

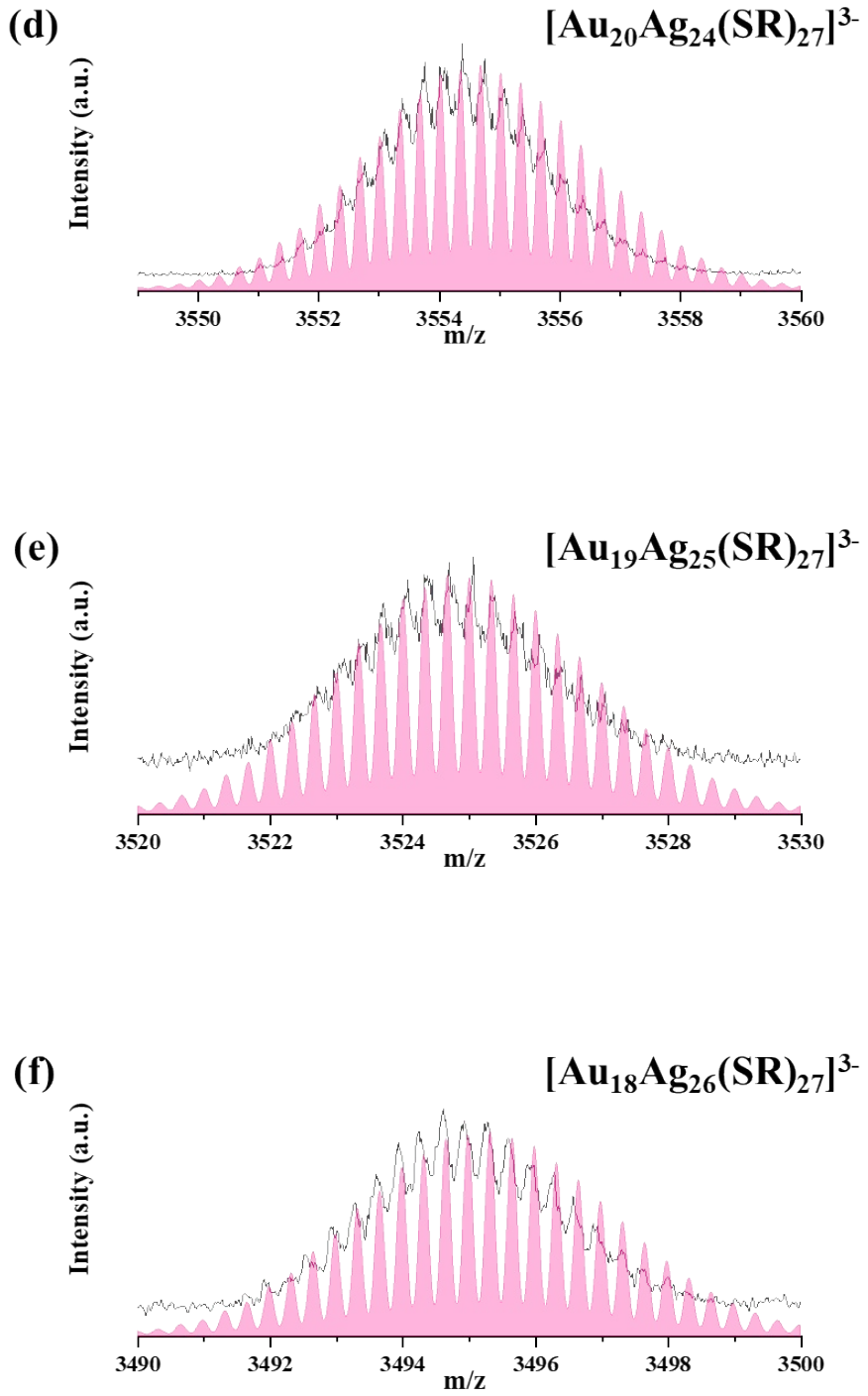

Figure S5. Experimental (black lines) and simulated (pink lines) isotope patterns of $[Au_xAg_{44-x}(SR)_{27}]^{3-}$ (x = 18-23) NCs.

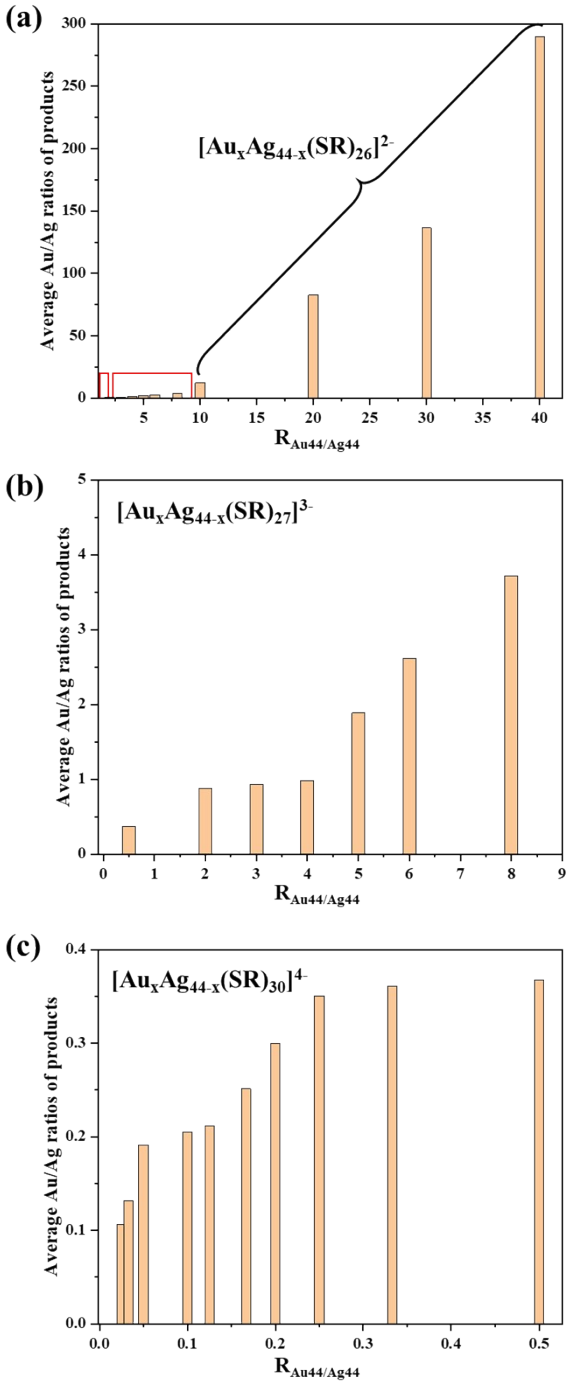

Figure S6. (a) The correlation between feeding Au_{44}/Ag_{44} ratios and average Au/Ag ratios of products. (b) The zoom-in view of the boxed area (with a feeding Au_{44}/Ag_{44} ratios of 0 to 0.5). (c) The zoom-in view of the boxed area (with a feeding Au_{44}/Ag_{44} ratios of 0.5 to 8).

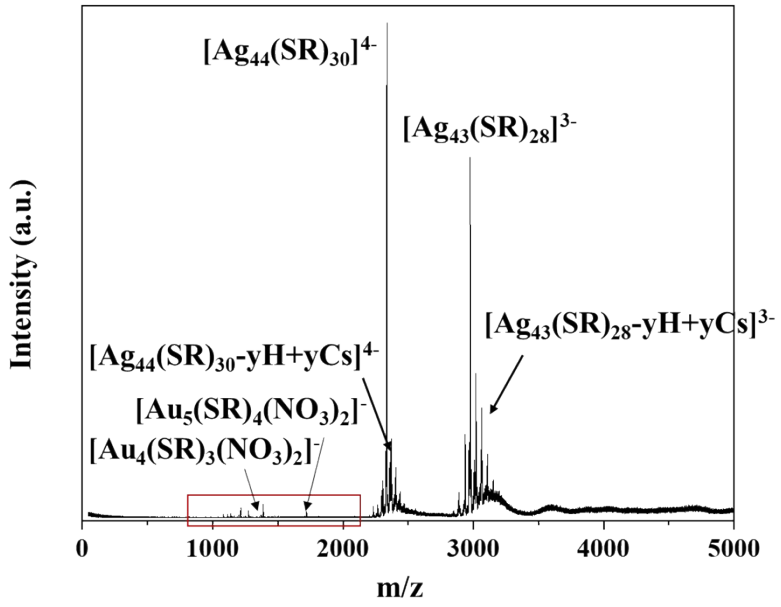

Figure S7. ESI mass spectrum of the reaction between $[Au_{44}(SR)_{26}]^{2-}$ and $[Ag_{44}(SR)_{30}]^{4-}$ ($R_{Au44/Ag44}$ = 1/3) at the reaction time (t) of 2 min.

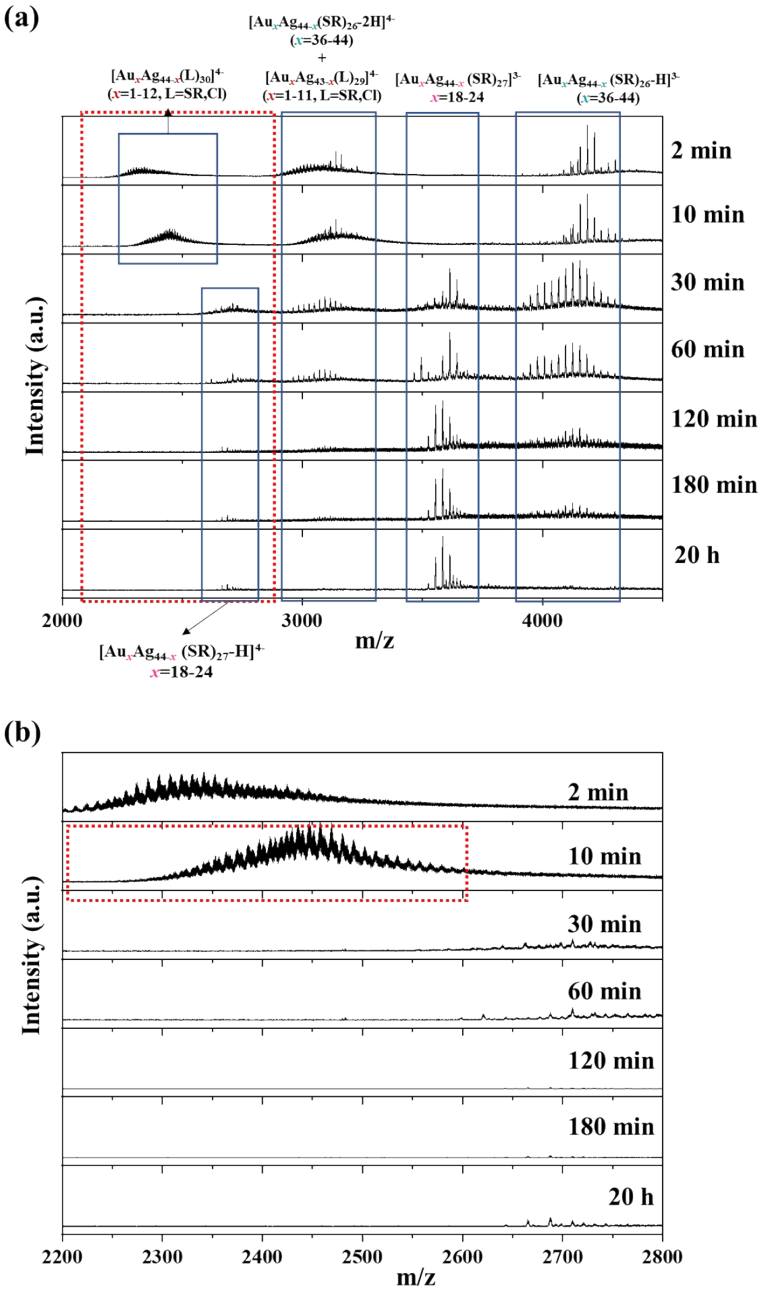
(a)
[Au$_x$Ag$_{44-x}$(SR)$_{26}$-2H]$^{4-}$
(x=36-44)
+
[Au$_x$Ag$_{44-x}$(L)$_{30}$]$^{4-}$
(x=1-12, L=SR,Cl)
[Au$_x$Ag$_{43-x}$(L)$_{29}$]$^{4-}$
(x=1-11, L=SR,Cl)
[Au$_x$Ag$_{44-x}$ (SR)$_{27}$]$^{3-}$
x=18-24
[Au$_x$Ag$_{44-x}$ (SR)$_{26}$-H]$^{3-}$
(x=36-44)
2 min
10 min
30 min
60 min
120 min
180 min
20 h
Intensity (a.u.)
2000
3000
4000
m/z
[Au$_x$Ag$_{44-x}$ (SR)$_{27}$-H]$^{4-}$
x=18-24
(b)
2 min
10 min
30 min
60 min
120 min
180 min
20 h
Intensity (a.u.)
2200
2300
2400
2500
2600
2700
2800
m/z

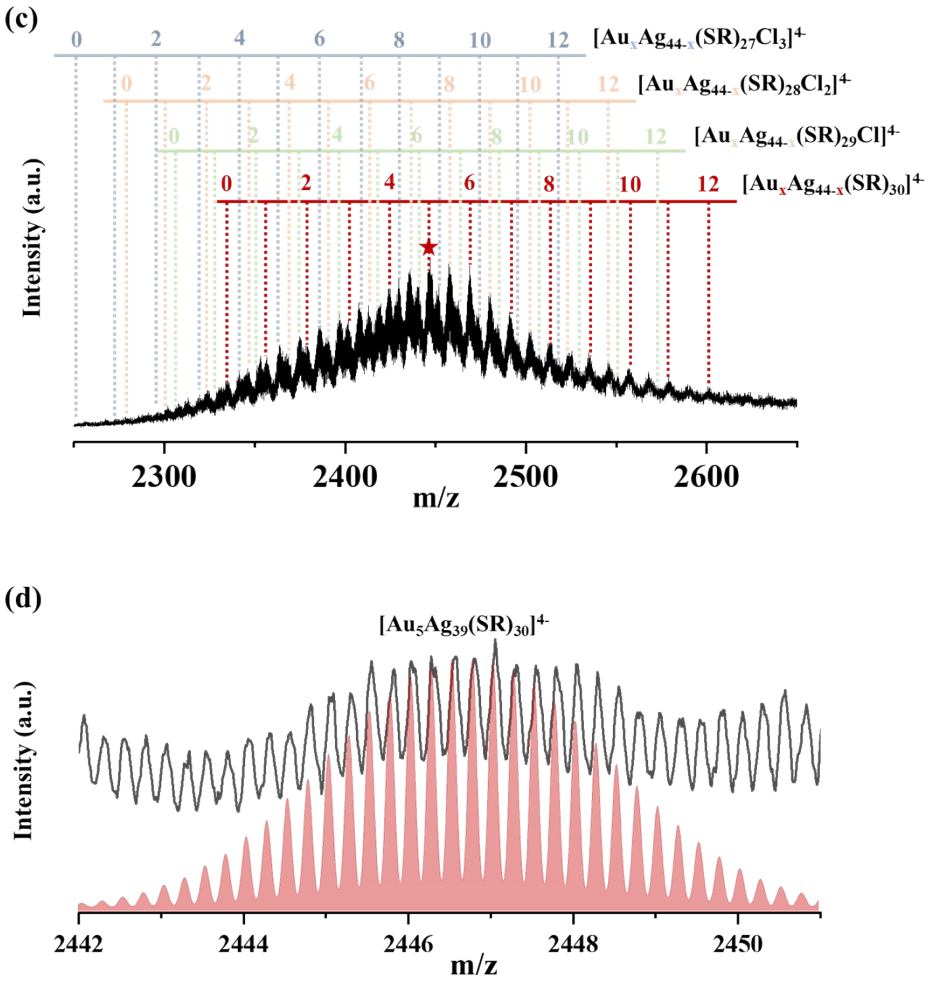

Figure S8. Time-course ESI mass spectra of the reaction between $[Au_{44}(SR)_{26}]^{2-}$ and $[Ag_{44}(SR)_{30}]^{4-}$ ($R_{Au44/Ag44}$ = 3/1) in the *m/z* range of (a) 2000-4500 and (b) 2200-2800. (c) The formula assignment for those peaks in the *m/z* range of 2200-2800 at t = 10 min. (d) Experimental (black lines) and simulated (red lines) isotope patterns of $[Au_5Ag_{39}(SR)_{30}]^{4-}$ (this peak was selected from (c), labeled by a red asterisk).

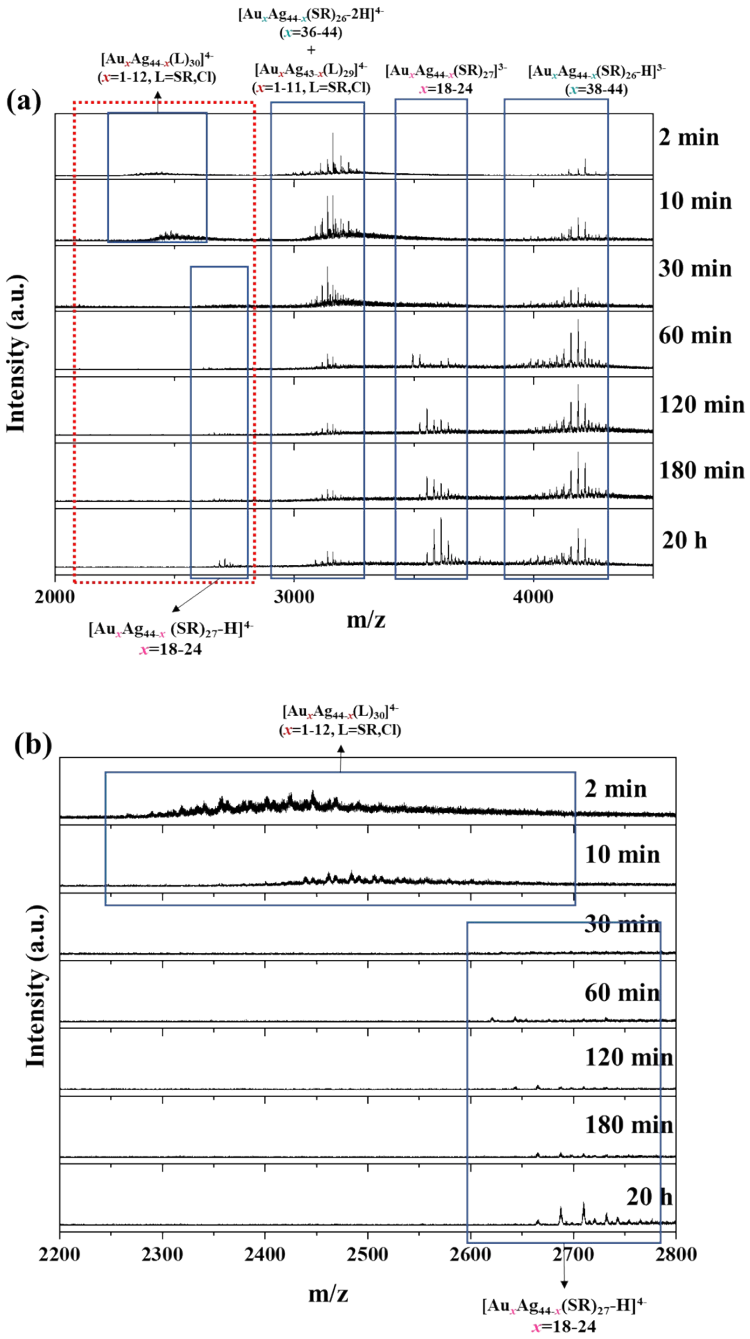

Figure S9. Time-course ESI mass spectra of the reaction between $[Au_{44}(SR)_{26}]^{2-}$ and $[Ag_{44}(SR)_{30}]^{4-}$ ($R_{Au44/Ag44}$ = 6/1) at the m/z range of (a) 2000-4500 and (b) 2200-2800.

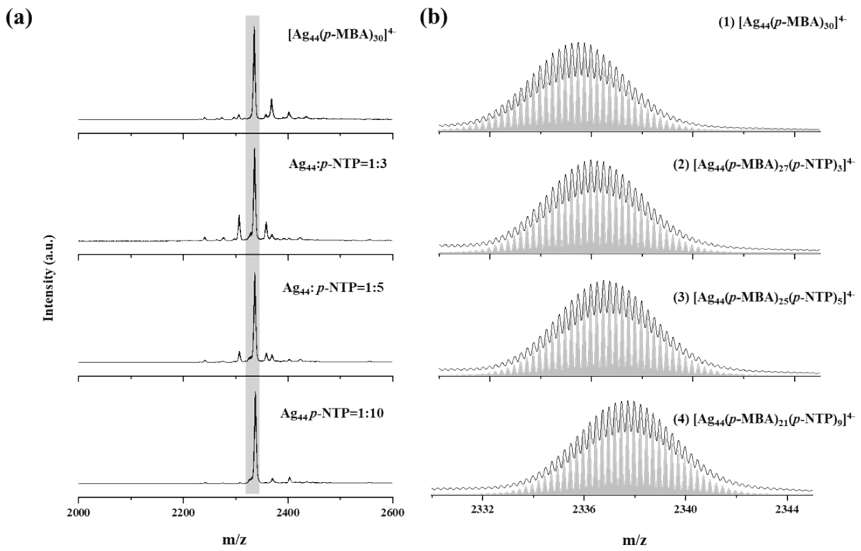

Figure S10. Ligand exchange of $[Ag_{44}(p\text{-MBA})_{30}]^{4-}$ with *p*-NTP at different ratios. (a) The mass spectrum in *m/z* range from 2000 to 2600. (b) The zoom-in of the box area of each corresponding panel with *m/z* from 2330 to 2344.

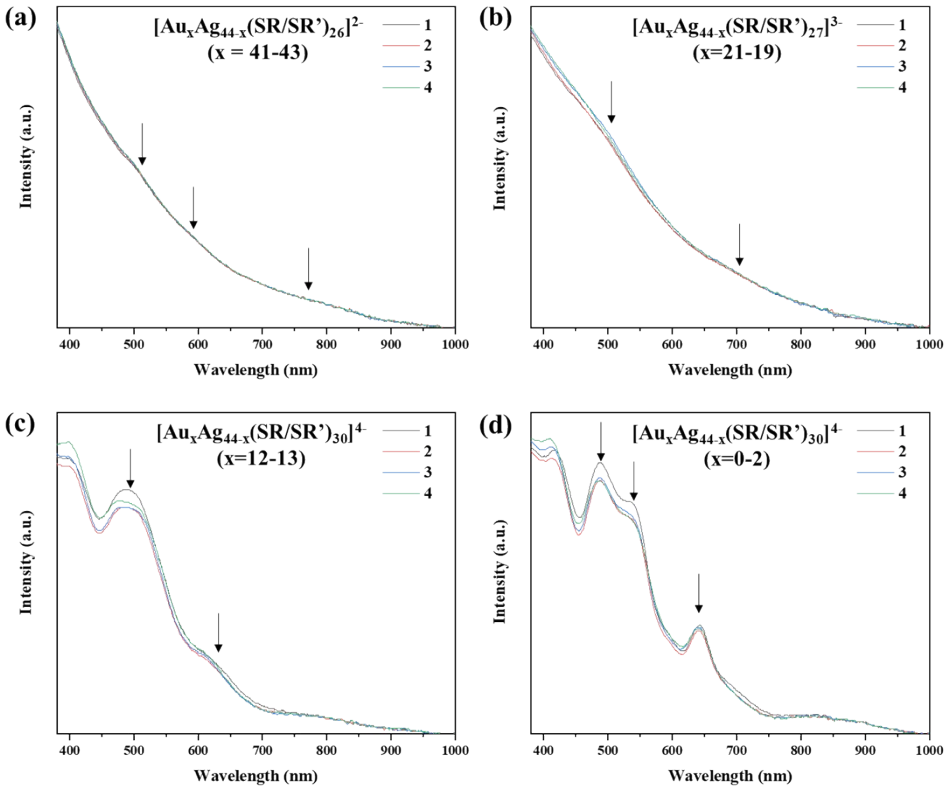

Figure S11. UV-Vis spectra of intercluster reactions between bi-ligand $[Ag_{44}(p\text{-MBA}/p\text{-NTP})_{30}]^{4-}$ and $[Au_{44}(p\text{-MBA})_{26}]^{2-}$ at different ratios to generate bi-ligand alloy NCs of (a) $[Au_xAg_{44-x}(SR/SR')_{26}]^{2-}$ (x = 41-43), (b) $[Au_xAg_{44-x}(SR/SR')_{27}]^{3-}$ (x = 19-21), (c) $[Au_xAg_{44-x}(SR/SR')_{30}]^{4-}$ (x = 12-13), and (d) $[Au_xAg_{44-x}(SR/SR')_{30}]^{4-}$ (x = 0-2).

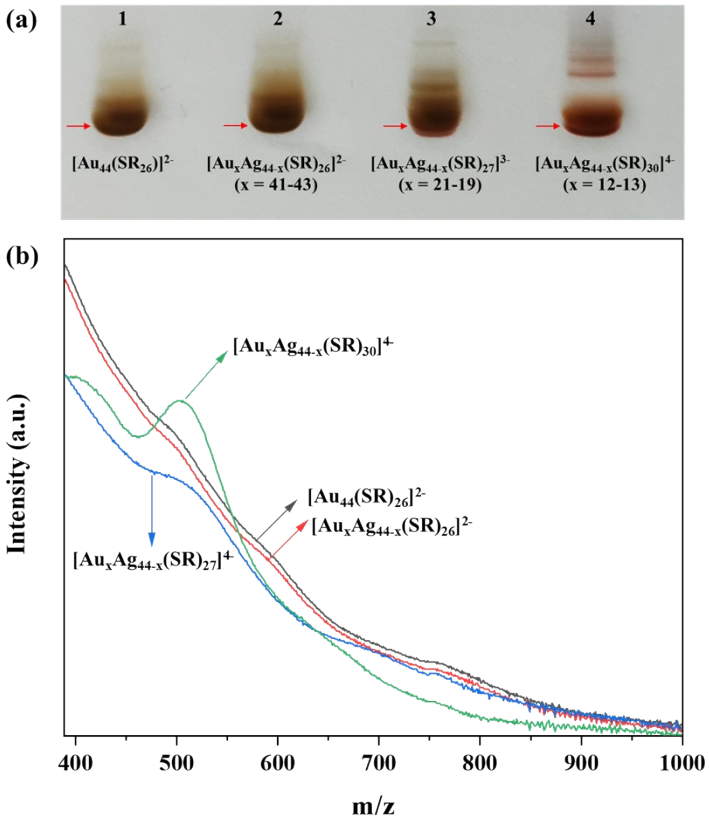

Figure S12. (a) Digital photo of the PAGE bands of the Au NCs and the Au/Ag alloy NCs. (b) The UV-Vis spectrum of $[Au_{44}(SR)_{26}]^{2-}$, $[Au_xAg_{44-x}(SR)_{26}]^{2-}$, $[Au_xAg_{44-x}(SR)_{27}]^{3-}$and $[Au_xAg_{44-x}(SR)_{30}]^{4-}$ after PAGE separation.

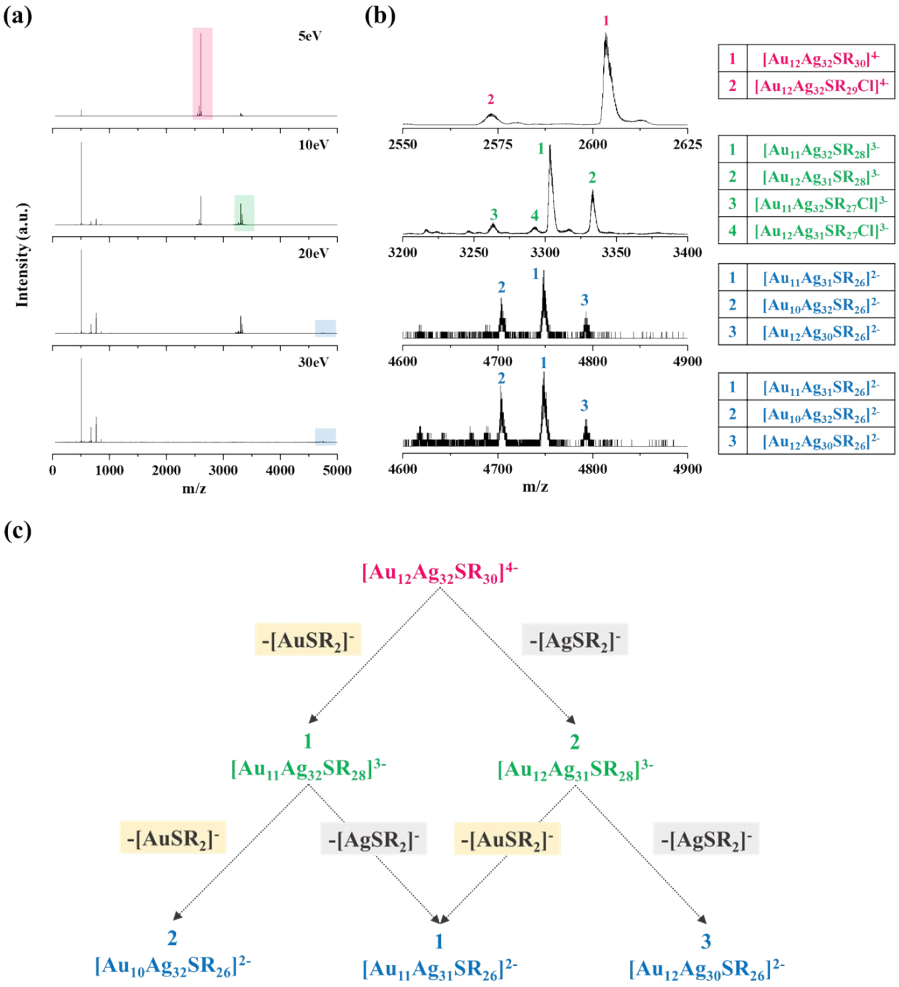

Figure S13. (a) Tandem mass spectra of $[Au_{12}Ag_{32}(SR)_{30}]^{4-}$ with m/z = 2602.5 at varied collision energies. (b) Zoom-in spectra of the boxed area in corresponding panel. (c) fragmentation process of $[Au_{12}Ag_{32}(SR)_{30}]^{4-}$ with m/z = 2602.5 in tandem mass spectrometry analysis.

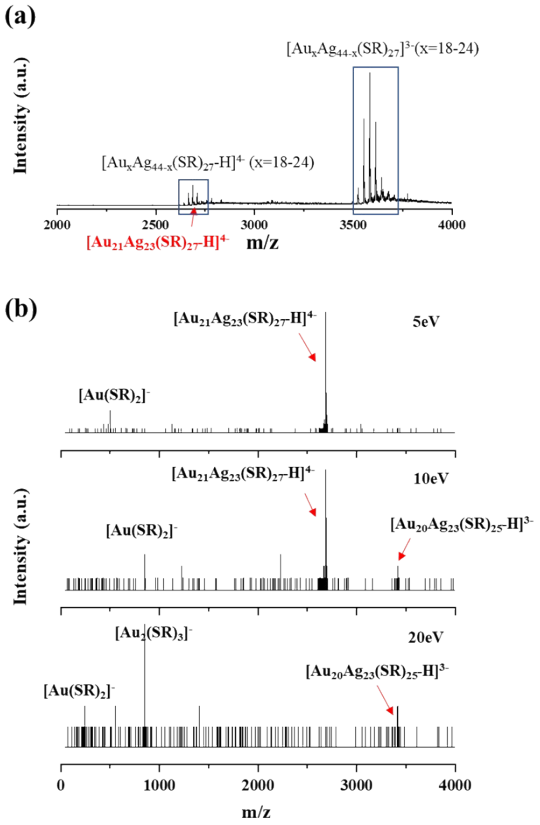

Figure S14. (a) ESI mass spectrum of $[Au_xAg_{44-x}(SR)_{27}]^{3-}$ NCs. (b) Tandem mass spectra of $[Au_{21}Ag_{23}(SR)_{27}\text{-}H]^{4-}$ with m/z = 2687.75 at varied collision energies.

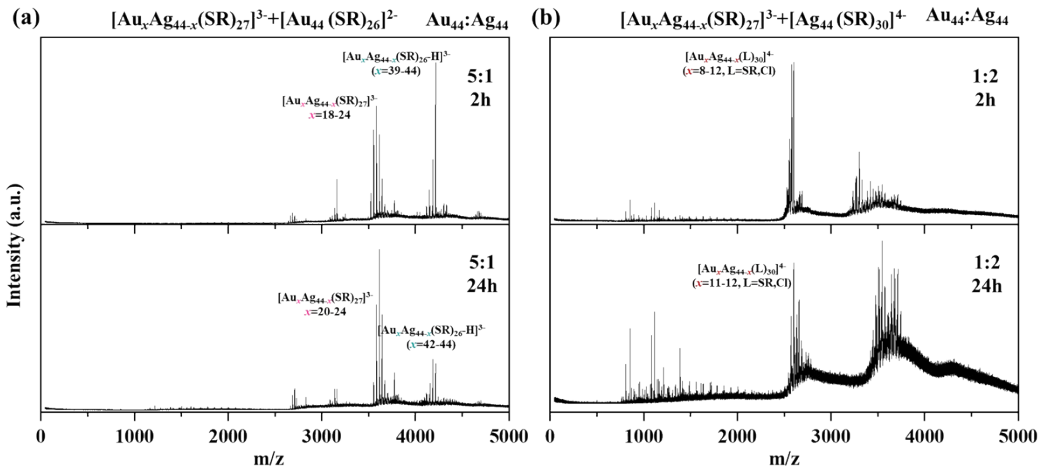

Figure S15. (a) Broad-range ESI mass spectra of the reactions between $[Au_xAu_{44-x}(SR)_{27}]^{3-}$ and $[Au_{44}(SR)_{26}]^{2-}$ (t = 2 and 24 h, $R_{Au44/Ag44}$ = 5/1). (b) Broad-range ESI mass spectra of the reactions between $[Au_xAu_{44-x}(SR)_{27}]^{3-}$ and $[Ag_{44}(SR)_{30}]^{2-}$ (t = 2 and 24 h, $R_{Au44/Ag44}$ = 1/2).

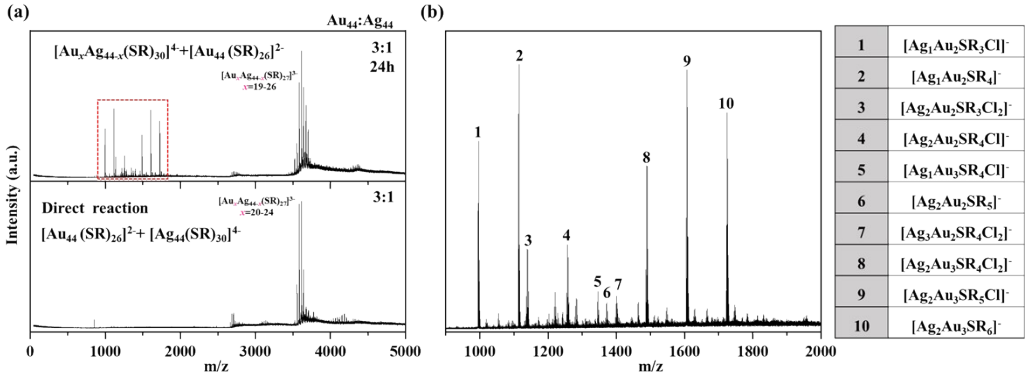

Figure S16. (a) Broad-range ESI mass spectra of the final products of inter-cluster reaction between $[Au_xAg_{44-x}(SR)_{30}]^{4-}$ and $[Au_{44}(SR)_{26}]^{2-}$ (top panel), and direct reaction between $[Ag_{44}(SR)_{30}]^{4-}$ and $[Au_{44}(SR)_{26}]^{2-}$ (bottom panel) at $R_{Au44/Ag44}$ = 3/1. (b) Zoom-in ESI mass spectra of the inter-cluster reaction between $[Au_xAg_{44-x}(SR)_{30}]^{4-}$ and $[Au_{44}(SR)_{26}]^{2-}$ at the *m/z* range of 900-2000. The right panel in (b) shows the molecular formulae of the labeled peaks.

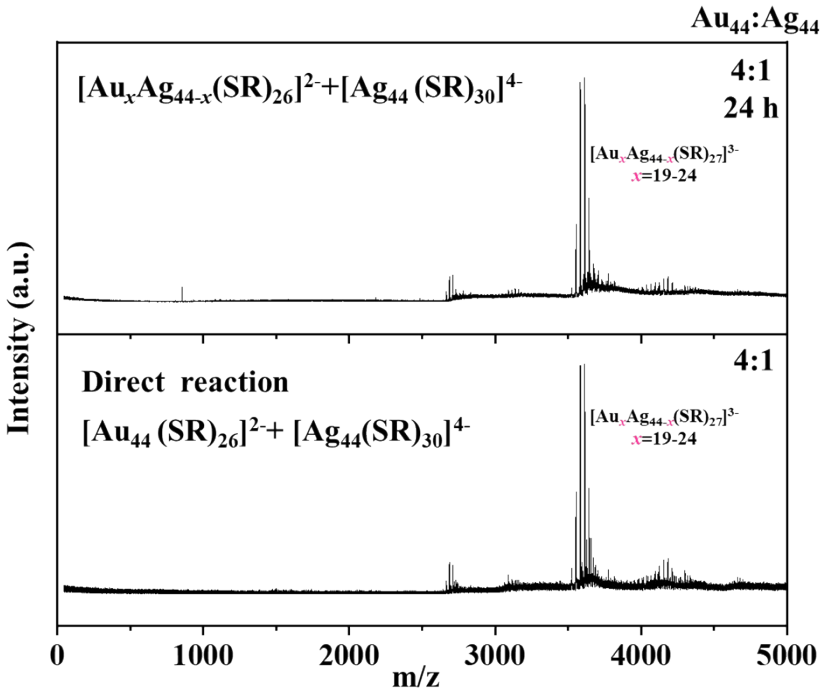

Figure S17. (a) ESI mass spectra of the final products of the inter-cluster reaction between $[Au_xAg_{44-x}(SR)_{26}]^{2-}$ and $[Ag_{44}(SR)_{30}]^{4-}$ (top panel), and direct reaction between $[Ag_{44}(SR)_{30}]^{4-}$ and $[Au_{44}(SR)_{26}]^{2-}$ at $R_{Au44/Ag44}$ = 4/1.

Table S1 Average feeding valence electrons in the inter-cluster alloy reactions and the corresponding alloy NCs products

Au_{44}:Ag_{44}	Average feeding electrons	Alloy NCs	Valence electrons
1:40	18.0		
1:30	18.1		
1:20	18.1		
1:10	18.2		
1:8	18.2	$[Au_xAg_{44-x}(SR)_{30}]^{4-}$ (x=1-12)	18
1:6	18.3		
1:5	18.3		
1:4	18.4		
1:3	18.5		
1:2	18.7		
2:1	19.3		
3:1	19.5	$[Au_xAg_{44-x}(SR)_{27}]^{3-}$ (x=18-24)	
4:1	19.6		
5:1	19.7		
6:1	19.7		20
8:1	19.8		
10:1	19.8	$[Au_xAg_{44-x}(SR)_{26}]^{2-}$ (x=40-44)	
20:1	19.9		
30:1	19.9		
40:1	20.0		

Reference

1 Q. Yao, X. Yuan, V. Fung, Y. Yu, D. T. Leong, D. E. Jiang, J. Xie, *Nat. Commun.* **2017**, *8*, 927.

2 A. Desireddy, B. E. Conn, J. Guo, B. Yoon, R. N. Barnett, B. M. Monahan, K. Kirschbaum, W. P. Griffith, R. L. Whetten, U. Landman, T. P. Bigioni, *Nature* **2013**, *501*, 399